A Continuum Robot with Twin-Pivot Structure: The Kinematics and Shape Estimation

Zheshuai Yang, Laihao Yang(✉), Lu Xu, Xuefeng Chen, Yanjie Guo, Jinxin Liu, and Yu Sun

Xi'an Jiaotong University, Xi'an 710049, China
{yzs12138,godfather707}@stu.xjtu.edu.cn, yanglaihao@xjtu.edu.cn

Abstract. Continuum robot, unlike conventional rigid-link robots, has numerous numbers of degrees of freedom, enabling it to be applied for confined space works, such as minimally invasive surgery, safe robot/objective interactions, and in-situ aero-engine detection. This study presented a cable-driven continuum robot with twin-pivot structure, which poses smaller diameter-length-ratio and torsion resistance ability compared with conventional single-pivot structure, as well as the kinematics and shape estimation. The kinematics model of the twin-pivot continuum robot is established based on the assumption of piecewise constant curvature, with which the mapping between driving space and operation space are presented. Finally, a prototype of continuum robot system with single section is constructed to verify the validation of the kinematics model and study the shape estimation. Based on the constructed prototype, the shape estimation of the continuum robot with different payloads is performed. The comparative results suggest that relative error is less than 5% for total length of the single section without payload, verifying the validity of the kinematics model. The comparison between the results with different payloads indicate that the increasing payload will increase the relative error.

Keywords: Continuum robot · Twin-pivot · Kinematics model · Shape estimation

1 Introduction

Continuum robots, which are inspired by the snakes and elephant trunks in nature, show incomparable flexibility and unique adaptability to confined space that conventional rigid-link robots are unable to achieve [1, 2]. Owing to these properties, continuum robots have been widely used in minimally invasive surgery [3–5], nuclear reactor maintenance [6] and rescue [7], etc. Recently, continuum robots were applied to the field of aero-engine engineering, serving as a novel solution for in-situ aero-engines repair [8–11], which has aroused extensive interests.

According to the joint structure, most continuum robots can be classified into two categories: rigid backbone continuum robot and flexible backbone continuum robot [12, 13]. The rigid backbone continuum robots were extensively investigated [11, 13, 14], and

X.-J. Liu et al. (Eds.): ICIRA 2021, LNAI 13013, pp. 466–475, 2021.
https://doi.org/10.1007/978-3-030-89095-7_45

some successfully commercial cases were reported by OC robotics [15] and SIASUN [16]. However, because of the large diameter and rigid backbone, the application of rigid backbone continuum robots in the confined space works is restricted [12, 17]. On the contrary, the flexible backbone enables the minimization of the size of continuum robot and poses better accessibility in confined space works. However, the length of these robots is generally shorter than the rigid backbone ones, and the payloads are limited [10]. So far, it is still a tough task to develop a flexible backbone continuum robot with smaller diameter-length-ratio and larger load carrying capacity. In this paper, the twin-pivot structure is introduced, which minimizes the size of the continuum robot and reduces the twisting angle caused by weight of the robot arm.

Apart from the structural design, it is necessary to establish a kinematics model for continuum robot. Most of the kinematics model for the rigid backbone continuum robots are based on the D-H method, while this method cannot be directly applied to the kinematics modeling of flexible backbone continuum robots since these robots have no definite joints. The kinematics model of flexible ones is generally based on the assumption of piecewise constant curvature (PCC), where each section of robotic arm is assumed to be a constant arc [1, 18, 19]. This method greatly simplifies the kinematics model. Thus, it has been widely used. However, the PCC-based kinematics model ignores the effects of loads, gravity, and friction [20, 21], which leads to lower accuracy. To improve the accuracy of modeling, a comprehensive static model that considers the effects of friction, loads, etc. is reported in [10] and [20], which has achieved great improvement in the model accuracy. However, the statics model suffers the defects of complex iteration and large computation, which makes it difficult to implement in real-time control directly. Generally speaking, the PCC-based kinematics model is still a reliable and the most used modeling method in the field of continuum robotics because of the simple principle of modeling and low computation cost with an acceptable error.

In this paper, the prototype of single section continuum robot driven by four cables is studied. The kinematics model is established based on the assumption of PCC, which maps the relationship between drive space and operation space. Furthermore, the shape estimation of the prototype with/without payload is detected by the vision system to evaluate the motion accuracy of the continuum robot and the reliability of the kinematic model.

The remainder of this paper is organized as follows. Section 2 establishes the mechanical structure and kinematics model. In Sect. 3, the experimental platform is presented, and the shape estimation of the prototype is detected by vision system. The last section summarizes the whole paper and gives the conclusions.

2 Modeling

2.1 Structure of Continuum Robot

The twin-pivot structure reported in [12] has been proven to effectively reduce the twisting angle of the continuum robot. The structure of this continuum robot with two sections is shown in Fig. 1. Each section consists of several segments which are composed of disks and NiTi rods, and is driven by four even distributed cables. As shown in Fig. 1,

the four dots indicate the location of the cables which drive the 2nd section, thus, the cables of 2nd section will pass through 1st section.

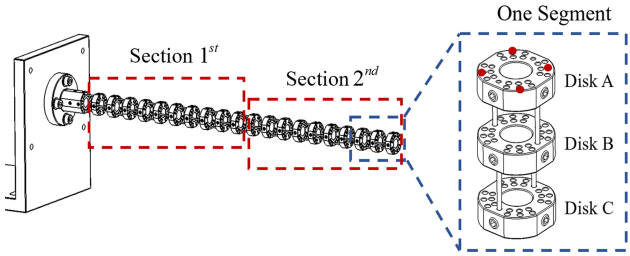

Fig. 1. The structure of the twin-pivot continuum robot.

2.2 Kinematics Model

Forward Kinematics. The purpose of the forward kinematics is to determine the tip position of the continuum robot based on the given lengths of cables. Since the continuum robot is composed of identical segment, the kinematic model is obtained, based on the analysis of a segment on which the joint coordinate system is shown in Fig. 2, and the joint parameters can be obtained from Table 1. According to these parameters, the homogeneous transformation matrix from coordinate system $\{i\}$ to $\{i+1\}$ can be written as:

$$ {}^{i-1}_{i}T = \mathrm{Rot}(x, \alpha_{i-1}) \cdot \mathrm{Trans}(a_{i-1}, 0, 0) \cdot \mathrm{Rot}(z, \theta_i) \cdot \mathrm{Trans}(0, 0, d_i) \tag{1} $$

where $i = 1, 2, 3$.

The forward kinematics of the segment can be written as:

$$ {}^{0}_{3}T = {}^{0}_{1}T \cdot {}^{1}_{2}T \cdot {}^{2}_{3}T \tag{2} $$

thus, the forward kinematics model of continuum robot can be written as:

$$ T = T_1 \cdot T_2 \cdot \ldots \cdot T_N \tag{3} $$

where N is the number of sections.

Inverse Kinematics. The purpose of the inverse kinematics is to determine the lengths of cables according to the known position. As shown in Fig. 3 and Fig. 4, taking the 1st

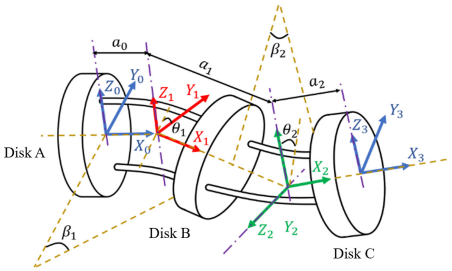

Fig. 2. The joint coordinate system of segment.

Table 1. The joint parameters.

Joint i	α_{i-1}	a_{i-1}	d_i	θ_i
1	0	$\frac{l_0}{\beta_1} \cdot \tan\frac{\beta_1}{2}$	0	$-\beta_1$
2	$\frac{\pi}{2}$	$\frac{l_0}{\beta_1} \cdot \tan\frac{\beta_1}{2} + h + \frac{l_0}{\beta_2} \cdot \tan\frac{\beta_2}{2}$	0	β_2
3	$-\frac{\pi}{2}$	$h + \frac{l_0}{\beta_2} \cdot \tan\frac{\beta_2}{2}$	0	0

section as an example, the lengths of the cables can be written as:

$$\begin{cases} \Delta l_{1,1} = \Delta l_{1,1}^1 = 2n_1\left[\left(\frac{l_0}{\beta_1} - r\cdot\cos\delta_1\right)\cdot\sin\frac{\beta_1}{2} + \left(\frac{l_0}{\beta_2} - r\cdot\sin\delta_1\right)\cdot\sin\frac{\beta_2}{2} - l_0\right] \\ \Delta l_{1,2} = \Delta l_{1,2}^1 = 2n_1\left[\left(\frac{l_0}{\beta_1} - r\cdot\sin\delta_1\right)\cdot\sin\frac{\beta_1}{2} + \left(\frac{l_0}{\beta_2} + r\cdot\cos\delta_1\right)\cdot\sin\frac{\beta_2}{2} - l_0\right] \\ \Delta l_{1,3} = \Delta l_{1,3}^1 = 2n_1\left[\left(\frac{l_0}{\beta_1} + r\cdot\cos\delta_1\right)\cdot\sin\frac{\beta_1}{2} + \left(\frac{l_0}{\beta_2} + r\cdot\sin\delta_1\right)\cdot\sin\frac{\beta_2}{2} - l_0\right] \\ \Delta l_{1,4} = \Delta l_{1,4}^1 = 2n_1\left[\left(\frac{l_0}{\beta_1} + r\cdot\sin\delta_1\right)\cdot\sin\frac{\beta_1}{2} + \left(\frac{l_0}{\beta_2} - r\cdot\cos\delta_1\right)\cdot\sin\frac{\beta_2}{2} - l_0\right] \end{cases} \tag{4}$$

where n_1 is the number of the segments in the 1st section.

The inverse kinematics model of the continuum robot can be then written as:

$$\Delta l_{i,j} = \sum_{k=1}^{i} \Delta l_{i,j}^k \tag{5}$$

where $\Delta l_{i,j}^k$ is the cable length of the j^{th} cable driving the i^{th} section at the k^{th} section, $i = 1, 2, \ldots, N$, and $j = 1, 2, 3, 4$.

The forward and inverse kinematics of the continuum robot can be expressed as Eq. (3) and Eq. (5), with which the mapping relationship between drive space and operation space is established.

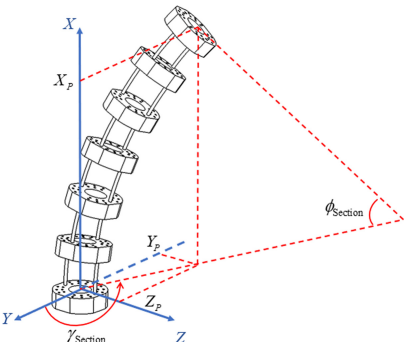

Fig. 3. Configuration of single section.

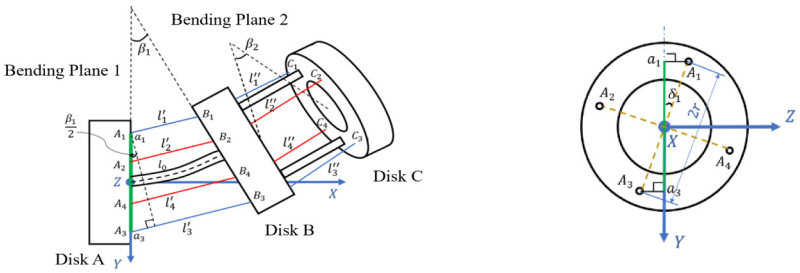

Fig. 4. (a) Configuration of segment; (b) Top view of disk A.

3 Shape Estimation

To verify the validation of the kinematics model, shape estimation is experimentally performed on a vision detection system. First of all, a prototype of single section cable-driven continuum robot is fabricated. Then the kinematic analysis and shape estimation experiments of the single section with or without payload in-plane are carried out.

3.1 Experimental Setup

As shown in Fig. 5, the experimental mainly consists of a continuum robot prototype, a vision system, pulleys, and motor units. The continuum robot prototype is fixed to an optical platform and driven by four cables which are controlled by four motor units. The pulleys are employed to change the directions of cables. In addition, the shape estimation in the *xoz* plane of the continuum robot could be detected by a vision system with a 5472 × 3648 pixel camera. By the way, the precision of the vision measuring system is 0.01 mm, which satisfies the shape estimation accuracy. It should be noted that the shape estimation is done by detecting the marked center point of each disk.

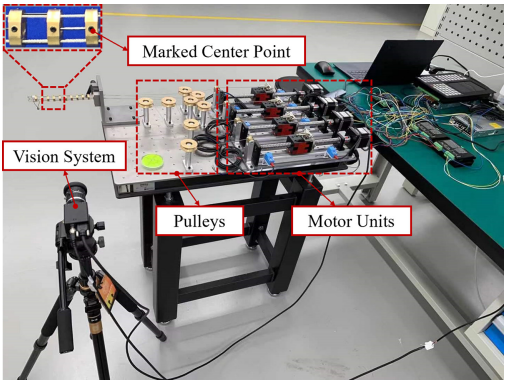

Fig. 5. The experimental platform.

As shown in Fig. 6, three continuum robot prototypes with different diameter-length-ratio (17/250, 17/200, and 17/150) are made, where each prototype contains 10 ten disks with a diameter of 17mm, and the only difference is the length of the NiTi rods. It is found that the diameter-length-ratio of 17/150 can better overcome the twist effect caused by gravity, thus, we choose this prototype (i.e. diameter-length-ratio of 17/150) for kinematics validation and shape estimation experiments.

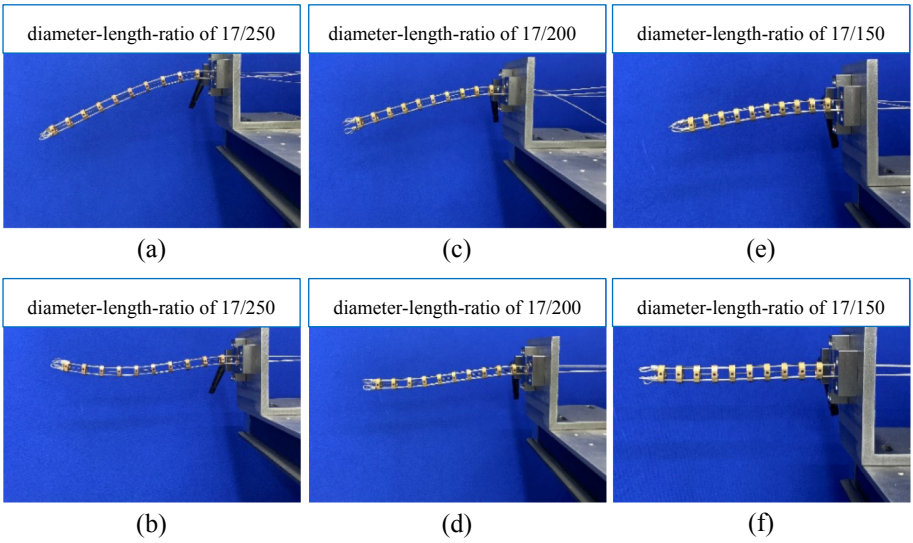

Fig. 6. (a) The prototype with diameter-length-ratio of 17/250 without cables constraint; (b) The prototype with diameter-length-ratio of 17/250 with cables constraint; (c) The prototype with diameter-length-ratio of 17/200 without cables constraint; (d) The prototype with diameter-length-ratio of 17/200 with cables constraint; (e) The prototype with diameter-length-ratio of 17/150 without cables constraint; (f) The prototype with diameter-length-ratio of 17/150 with cables constraint.

3.2 Shape Estimation of a Single Section

To evaluate the motion accuracy of the continuum robot and the reliability of the kinematic model, the shape of the single section is detected by the vision system. As shown in Fig. 7, the plane bending experiment ($\theta = 0°$ to 90°) without payload is carried out, and the total length of the prototype is 150 mm. Another two experiments with a payload of 51.3 g and 101.3 g are conducted, where the masses of the weights are 50 g and 100 g respectively, and the mass of the cable used to fix the weights is 1.3 g. The results are shown in Fig. 8 and Fig. 9, where the experimental data are represented by blue boxes and the kinematic-model-calculated data are represented by red stars. And the top position accuracy measurement results are shown in Table 2.

As shown in Fig. 7, the single section prototype is in good agreement with the kinematic model when the bending angle is 90°. By comparing the experimental and model-based data, the maximum error is 7.4 mm, which accounts for 4.9% of the entire length of the single section (i.e. 150 mm). In Fig. 8 and Fig. 9, due to the influence of the payload, the kinematics model is unable to accurately estimate the shape of the prototype, and the maximum errors are 14.91 mm and 23.38 mm, accounting for 9.94% and 15.59% of the entire section length.

3.3 Limitation Discussion

As shown in the comparative experimental results, to some degree, the kinematics model based on PCC can characterize the motion of the continuum robot within an acceptable error. However, since the assumption of PCC ignores the effects of gravity, payload, and friction, the simulation accuracy is limited, especially when the payload or the length of continuum robot is increased. In the coming future, the kinematic and static model which considers the mechanical characteristics of continuum robot and other methods [22, 23] will be further deduced to improve the motion accuracy and reliability. In addition, the FBG sensing-based shape reconstruction techniques will be applied to solve the kinematic modeling problems, since it is independent of the theoretical model and the shape of the continuum robot can be obtained in real-time [24].

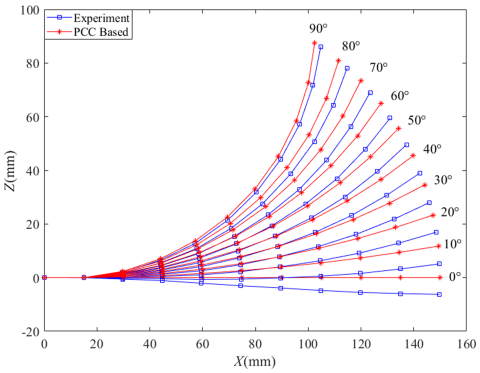

Fig. 7. A bending test without payload.

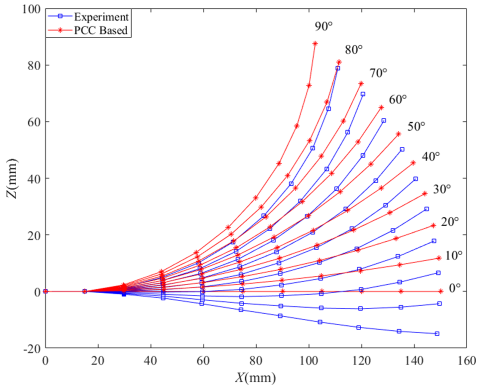

Fig. 8. A bending test with a payload of 51.3 g.

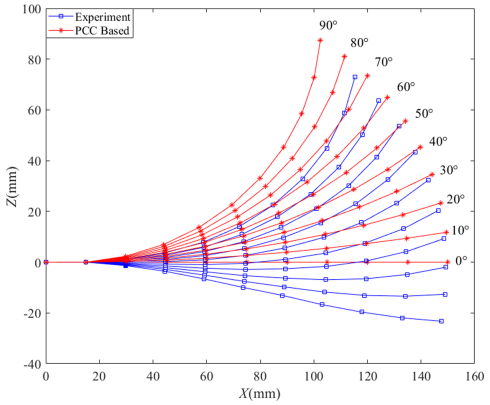

Fig. 9. A bending test with a payload of 101.3 g.

Table 2. Top accuracy measurement results

Bending angle (deg)	Desired position (mm)		Actual position without payload (mm)		Actual position with payload of 51.3 g (mm)		Actual position with payload of 101.3 g (mm)	
	X	Z	X	Z	X	Z	X	Z
0	150	0	149.78	−6.24	148.83	−14.91	147.59	−23.26
10	149.34	11.75	149.75	5.12	149.57	−4.32	149.02	−12.65
20	147.38	23.34	148.46	16.93	149.18	6.61	149.33	−1.96
30	144.16	34.61	145.95	27.99	147.60	17.84	148.44	9.23
40	139.71	45.39	142.20	38.90	144.76	29.13	146.38	20.31

(*continued*)

Table 2. (*continued*)

Bending angle (deg)	Desired position (mm)		Actual position without payload (mm)		Actual position with payload of 51.3 g (mm)		Actual position with payload of 101.3 g (mm)	
	X	Z	X	Z	X	Z	X	Z
50	134.13	55.55	137.21	49.53	140.68	39.82	142.72	32.36
60	127.50	64.95	131.03	59.47	135.36	50.18	137.84	43.45
70	119.91	73.47	123.45	69.04	128.59	60.40	131.75	53.74
80	111.54	81.00	114.76	78.13	120.69	69.63	124.24	63.59
90	102.47	87.47	104.80	86.17	110.08	78.84	115.36	72.98

4 Conclusions

In this paper, the kinematics model and shape estimation of the twin-pivot continuum robot are numerically and experimentally studied. First and foremost, an experimental platform consisting of a prototype, a vision system, pulleys, and motor units is presented. Then the kinematics model of prototype is established based on the assumption of PCC. Finally, the vision system is utilized to detect the shape of the continuum robot. With the estimated shape, the motion accuracy of the continuum robot and the reliability of the kinematic model are evaluated. The results suggest that the maximum error is 7.4mm, which accounts for 4.9% of the entire length of the single section. In addition, the payload tests are carried out, the comparative results indicates that the kinematics model accuracy for the cases with payload is restricted due to the limitation of PCC assumption.

The results show that the kinematic model is enabled to accurately estimate the shape of the prototype with an acceptable error, while the motion accuracy with the payload increasing. In the coming works, the payload performance of the continuum robot can be improved by optimizing the structure design and adding variable stiffness structure. In addition, a kinematics and statics model should be used to compensate the effect of the payload and the FBG sensing-based shape reconstruction techniques will be applied to solve the kinematic modeling problems.

Acknowledgements. This work is sponsored by the National Natural Science Foundation of China (Nos. 52105117, 91860127).

References

1. Webster, R.J., Jones, B.A.: Design and kinematic modeling of constant curvature continuum robots: a review. Int. J. Robot. Res. **29**(13), 1661–1683 (2010)
2. Hannan, M.W., Walker, I.D.: Kinematics and the implementation of an elephant's trunk manipulator and other continuum style robot . Robot Syst. **20**(2), 45–63 (2003)

3. Ji, D., Kang, T.H., Shim, S., et al.: Analysis of twist deformation in wire-driven continuum surgical robot. Int. J. Control Autom. Syst. **18**(1), 10–20 (2019)
4. Shin, W.H., Kwon, D.S.: Surgical robot system for single-port surgery with novel joint mechanism. IEEE Trans. Biomed. Eng. **60**(4), 937–944 (2013)
5. Camarillo, D.B., Carlson, C.R., Salisbury, J.K.: Configuration tracking for continuum manipulators with coupled tendon drive. IEEE Trans. Rob. **25**(4), 798–808 (2009)
6. Buckingham, R., Graham, A.: Nuclear snake-arm robots. Ind. Robot Int. J. **39**(1), 6–11 (2012)
7. Kamegawa, T., Yamasaki, T., Igarashi, H., et al.: Development of the snake-like rescue robot "KOHGA. In: 2004 IEEE International Conference on Robotics and Automaton on Proceedings, pp. 5081–5086. IEEE, New York (2004)
8. Dong, X., Palmer, D., Axinte, D., et al.: In-situ repair/maintenance with a continuum robotic machine tool in confined space. J. Manuf. Process. **38**, 313–318 (2019)
9. Dong, X., Axinte, D., Palmer, D., et al.: Development of a slender continuum robotic system for on-wing inspection/repair of gas turbine engines. Robot. Comput. Integr. Manuf. **44**, 218–229 (2017)
10. Wang, M., Dong, X., Ba, W., et al.: Design, modelling and validation of a novel extra slender continuum robot for in-situ inspection and repair in aeroengine. Robot. Comput.-Integr. Manuf. **67**, 102054 (2021)
11. Tang, L., Wang, J., Zheng, Y., et al.: Design of a cable-driven hyper-redundant robot with experimental validation. Int. J. Adv. Robot. Syst. **14**(5), 1–12 (2017)
12. Dong, X., Raffles, M., Cobos-Guzman, S., et al.: A novel continuum robot using twin-pivot compliant joints: design, modeling, and validation. J. Mech. Robot.-Trans. ASME **8**(2), 021010 (2016)
13. Xu, W., Liu, T., Li, Y.: Kinematics, dynamics, and control of a cable-driven hyper-redundant manipulator. IEEE/ASME Trans. Mechatron. **23**(4), 1693–1704 (2018)
14. Tang, L., Huang, J., Zhu, L., et al.: Path tracking of a cable-driven snake robot with a two-level motion planning method. IEEE/ASME Trans. Mechatron. **24**(3), 935–946 (2019)
15. Bogue, R.: Snake robots a review of research, products and applications. Ind. Robot-Int. J. **41**(3), 253–258 (2014)
16. SIASUN. http://www.siasun.hk/. Accessed 16 Apr 2021
17. Dong, X., Raffles, M., Guzman, S.C., et al.: Design and analysis of a family of snake arm robots connected by compliant joints. Mech. Mach. Theory **77**, 73–91 (2014)
18. Renda, F., Giorelli, M., Calisti, M., et al.: Dynamic model of a multibending soft robot arm driven by cables. IEEE Trans. Robot. **30**(5), 1109–1122 (2014)
19. Garriga-Casanovas, A., Rodriguez, Y., Baena, F.: Kinematics of continuum robots with constant curvature bending and extension capabilities. J. Mech. Robot. **11**(1), 011010 (2019)
20. Yuan, H., Zhou, L., Xu, W.: A comprehensive static model of cable-driven multi-section continuum robots considering friction effect. Mech. Mach. Theory **135**, 130–149 (2019)
21. Xu, K., Simaan, N.: Analytic formulation for kinematics, statics, and shape restoration of multibackbone continuum robots via elliptic integrals. J. Mech. Robot.-Trans. ASME **2**(1), 13 (2010)
22. Barrientos-Diez, J., Dong, X., Axinte, D., et al.: Real-time kinematics of continuum robots: modelling and validation. Robot. Comput.-Integr. Manuf. **67**, 12 (2021)
23. Bieze, T.M., Kruszewski, A., Carrez, B., et al.: Design, implementation, and control of a deformable manipulator robot based on a compliant spine. Int. J. Robot. Res. **39**(14), 1604–1619 (2020)
24. Shi, C., Luo, X., Qi, P., et al.: Shape sensing techniques for continuum robots in minimally invasive surgery: s survey. IEEE Trans. Biomed. Eng. **64**(8), 1665–1678 (2017)